In Vitro Measurement of Strain Localization Preceding Dissection of the Aortic Wall Subjected to Radial Tension

M Di Giuseppe, M Zingales, S Pasta, S Avril

Experimental Mechanics
https://doi.org/10.1007/s11340-020-00641-1

SP ISS: EXPERIMENTAL ADVANCES IN CARDIOVASCULAR BIOMECHANICS

In Vitro Measurement of Strain Localization Preceding Dissection of the Aortic Wall Subjected to Radial Tension

M. Di Giuseppe[1] · M. Zingales[2] · S. Pasta[2] · S. Avril[3]

Received: 31 January 2020 / Accepted: 20 July 2020

Abstract

Background Aortic dissection (AD) is a common pathology and challenging clinical problem. A better understanding of the biomechanical effects preceding its initiation is essential for predicting adverse events on a patient-specific basis. Moreover, the predictability of patient-specific biomechanics-based computational models is hampered by uncertainty about boundary conditions and material properties.

Objective Predisposition of thoracic aortic aneurysms (TAA) to ADs can be related to the degradation of biomechanically important constituents in the aortic wall of TAAs. The goal of the present study is to develop a new methodology to measure strain fields in aortic tissues subjected to radial tensile loading, combining optical coherence tomography (OCT) and digital image correlation (DIC).

Methods Radial tensile tests are performed on 5 samples collected from a healthy porcine descending thoracic aorta and 2 samples collected from a human ascending thoracic aortic aneurysm. At each step of the radial tensile test, the OCT technique is used to acquire images of the sample presenting a speckle pattern generated by the optical signature of the tissue. The speckle pattern is used to quantify displacement and strain fields using DIC. Stress-strain data are also measured throughout the analyzed range.

Results Results show that strain commonly localizes very early during tensile tests, at the location where the crack onset occurs. Aneurysm samples even show a sharper localization than healthy porcine tissues.

Conclusion This suggests the importance of extending the analysis to a larger number of human samples using our new methodology to better identify the conditions predisposing aortas to dissection.

Keywords Aortic dissection · Optical coherence tomography · Digital image correlation · Radial tensile test · Strain field · Radial stiffness

Introduction

Aortic dissection (AD) is an adverse condition of the aorta, which is typically described by a primary intimal tear on the aortic wall [1]. Dissections are commonly described as first propagating in the radial direction towards the medial layer, then it proceeds within the media, or between the media and the adventitia, causing the layers of the aortic wall to separate [2]. The separation allows the blood flow to enter the aortic wall, where a secondary channel, a so-called false lumen, is created. This leads to dilation and weakening of the wall of the false lumen with increasing probability of fatal rupture, bleeding or malperfusion [3, 4]. In the absence of intervention, acute aortic dissections have a mortality risk upon 90% with the majority of deaths occurring within 48 h [5]. The incidence of spontaneous aortic dissections is reported to be 5–30 cases per million people per year and strongly depends on the presence of risk factors.

Although arterial dissection is a common pathology and a challenging clinical problem, the underlying biomechanics remain underexplored. The structural organization is prone

✉ S. Avril
avril@emse.fr

[1] Department of Health Promotion, Mother and Child Care, Internal Medicine and Medical Specialties, University of Palermo, 90128 Palermo, Italy

[2] Department of Engineering, University of Palermo, Viale delle Scienze, Ed.8, 90128 Palermo, Italy

[3] Mines Saint-Étienne, Univ Lyon, Univ Jean Monnet, INSERM, U1059 SAINBIOSE, 158 cours Fauriel, 42023 Saint-Etienne cedex 2, France

Published online: 11 August 2020

to separation in a plane parallel to the lumen [6, 7], as elastin fibers, collagen bundles and smooth muscle cells are organized in concentric lamellar units in the media layer [8].

Hypertension is the most common predisposing factor to AD [1, 9]. AD is frequent in patients harboring a thoracic aortic aneurysm (TAA). TAA is a life-threatening cardiovascular disease leading to weakening of the aortic wall and permanent dilation [10]. TAA is characterized at the tissue level by extracellular matrix degradation and biomechanical weakening of the aortic wall, ultimately leading to dilation and failure by rupture or dissection. The mortality of thoracic aneurysms is estimated to be 50% over 5 years [11]; nevertheless, AD can occur in the absence of an aortic dilatation [12].

Predisposition of TAAs to ADs can be related to the degradation of the aortic wall in TAAs. A better understanding of the biomechanical effects preceding dissection initiation is essential for predicting such an adverse event on patient-specific basis. Moreover, the predictability of patient-specific biomechanics-based computational models is hampered by uncertainty about boundary conditions and material properties in such complex situations [13–17]. Experimental studies that focused on ADs permitted to measure strength of dissecting aortic tissues [18–22] subjected to radial tension. Although the radial stress in an elastic cylinder subjected to an inflating pressure is negative, the radial stress can become positive in the aortic wall and possibly induce AD when glycosaminoglycans (GaGs) accumulate in the wall [23, 24]. However, to the best of our knowledge, the strain distribution across the aortic wall preceding a dissection has never been measured.

Optical coherence tomography (OCT) is an imaging modality of micrometric scale permitting the visualization of tissue microstructure at different sub-surface levels (high-resolution and cross sectional images acquisition with a near-infrared light) [25–30].

OCT has been used for medical application studies (*in vivo*) and for bioengineering research (*in vitro*) to characterize soft and hard human tissues. This technique can be applied to quantify the mechanical properties of biological tissues [31, 32]. In experimental biomechanics, OCT can be potentially combined with digital image correlation (DIC) to perform material characterization by measurements of displacements and strains [32, 33]. Originating from experimental mechanics, DIC has now been applied in several scientific fields including biomechanics [32, 34–37]. In fact, DIC has been largely adopted to study the mechanical behavior of biological tissues because it offers non-contact full-field measurements, which are beneficial when studying anisotropic and inhomogeneous materials such as cardiovascular tissues [38, 39]. DIC usually requires an artificial speckle pattern to be applied to the object surface and tracked during deformation [36]. More importantly, the speckle quality strongly affects the success and accuracy of DIC analysis [40]. Ensuring appropriate speckle quality can be very challenging in soft tissues because of the moist and reflective surface. Different studies have been conducted so far using DIC to characterize the mechanical and structural properties of aortic tissue [41]. Regarding the aorta, few studies have applied the OCT technique [28, 42]. This scarcity of OCT studies on the aortic tissue can be explained by the main limitations of OCT, which are its penetration depth and image contrast. The penetration depth across the aorta is usually less than 500 μm for state-of-the-art commercially available OCT systems operating in the 1.3 μm wavelength range [9], whereas human or porcine aortas have a thickness of about 2 mm. These limitations of OCT are related to the scattering properties of biological tissues. To overcome these limitations, it is possible to apply a tissue clearing technique to increase the OCT imaging contrast and penetration capability [42, 43], although the clearing process can alter biomechanical properties of the aorta [44].

The goal of the present paper is to introduce a new methodology combining DIC and OCT to measure strain fields in aortic tissues subjected to tensile loading along the radial direction. We first describe the experimental protocol and apply it on healthy porcine tissues, then the methodology is extended to ATAA human tissues as a first proof of principle for the evaluation of dissection predisposition.

Methods

Porcine Tissue Origin

In this study, aortic samples were collected from different segment of the aorta (Fig. 1). A descending thoracic aorta was collected from a healthy pig. The Veterinary School of Lyon (Institut Claude Bourgelat) supplied the aortas in

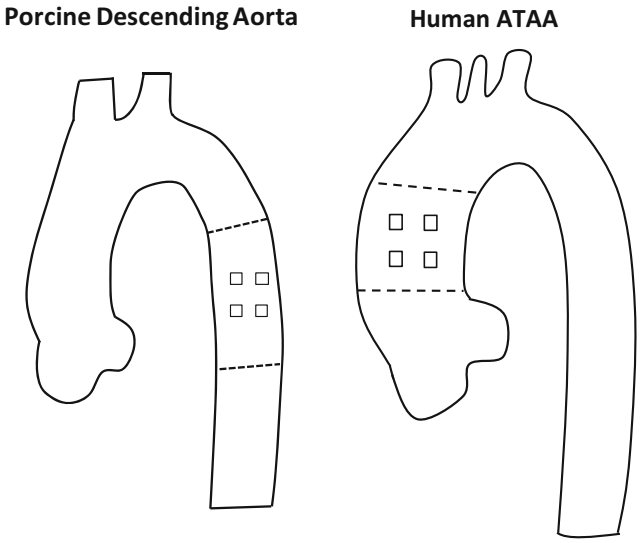

Fig. 1 Representation of the area of the aorta where samples were collected

accordance with the recommendations of the ethics committee of VetAgro Sup (C2EA No 18) and animal testing regulation – Directive 2010/63/EU. The study and protocol were reviewed and approved by the ethics committee of VetAgro Sup (project approved under No 1546). Porcine aortas were cryopreserved after collection and stored at −24 °C before experimental testing.

Human ATAA Tissue Origin

An ascending thoracic aortic aneurysm was collected from a patient undergoing elective surgery. The collection of the ATAA tissue was carried out in accordance with guidelines of the Institutional Review Board of the University Hospital Center of Saint-Etienne, and the patient signed informed consent before surgery. The human tissue was cryopreserved after collection in a physiological saline solution and stored at −24 °C before material testing.

Sample Preparation

Both the human pathological and healthy animal tissues underwent the same process to prepare samples for mechanical testing. The aortic samples were cut along the axial direction to obtain flat rectangular tissue sheets, and the loose connective tissues was carefully removed from the adventitial side. From the healthy tissue, a total of 5 square samples ($5x5mm^2$) were cut, whereas 2 square samples of the same size ($5x5mm^2$) were cut from the human pathological tissue.

Uniaxial Testing

Mechanical characterization of the aortic tissue was performed on a previously developed OCT experimental setup [42], which was adapted for short biological samples (Fig. 2). Specifically, the grips were substituted with L-shaped 3D printed arms anchored onto the device. We assumed that the force measured with a load cell in the arm was entirely transmitted through all parts of the system (arms, glue, sample) and that it induced a uniform stress in the arterial sample regardless the effects of stiffness of all other components of the system.

Samples were glued to a 3D printed arm using cyanoacrylate glue, with sandpaper placed between the arm and the sample. The arm was then mounted on the device with the transverse section of the sample perpendicular to the OCT camera; glue was placed on the other arm and a compression force of 0.5 N was gently applied for 10 min to allow adhesive curing. After the gluing process, the sample was rehydrated by filling the testing chamber with 0.9% physiological saline solution at room temperature. Due to the gentle compression, the tests always started with negative offset in the force values, which was eventually removed for the analysis. Figures 3 and 4 show a schematic of the tested samples with the 3 vectors of the cartesian reference frame and a picture of the sample before and after rupture.

During each test, we decided to manually apply in each direction twelve displacement steps of 0.01 mm ± uncertainty as this corresponds to an average strain of 0.005 (0.5%). Indeed, samples were collected from the same area and had an average thickness of 2 mm.

Steps were applied acting on the micrometric linear stages Newport M-460P-X (Fig. 2), while continuously acquiring corresponding load values with a load cell of 22 N capacity (rate output ±1.57 mV/V) with an accuracy of about 0.1 N, conditioned with a Futek IPM650 panel mount display (input range up to ±500 mV/V). After the last step, the sample was stretched up to rupture dynamically applying a strain rate of 0.1 s^{-1} to verify that the failure did not occur in the bond where the sample was glued to the arm; this quite large rate was due to technical constraint but it did not affect the main results of the study.

Between each displacement step, there was a time window of about 30s requested to acquire the images with the OCT system.

Data Analysis

From force values obtained by the load cell for porcine samples, the stress was calculated. The stress-strain data were fitted by polynomial functions using SigmaPlot (Systat Software Inc., San Jose, California). These functions were used to interpolate the stress values within the experimental displacement range. Stress-strain curves were plotted considering the engineering stress values σ_{xx}, that were calculated by dividing the measured force value by the initial cross-sectional area of the sample (5×5 mm^2), and the average Green-Lagrange strain across the sample.

Tissue stiffness defined as the first derivative of the stress-strain response at a given point was evaluated for porcine samples. Since all samples had the same thickness, we evaluated the stiffness at a displacement value of 0.04 mm, corresponding to an average strain of 0.01 (1%) (considering the strain values obtained by DIC), starting from the first positive stress point of the curve.

OCT–Acquisition System

For 3D volume image acquisition, the aortic wall reflectivity was measured with an OCT system (Thorlabs OCT-TEL220C1) [30]. System settings were as follows: a center wavelength of 1300 nm, lateral resolution 7 μm, focal length 18 mm, maximum sensitivity range 111 dB (at 5.5 kHz), imaging depth 2.6 mm (in water), axial resolution 4.2 μm in water and 5.5 μm in air. We found that PBS does not have different refractive properties compared to water, which has a

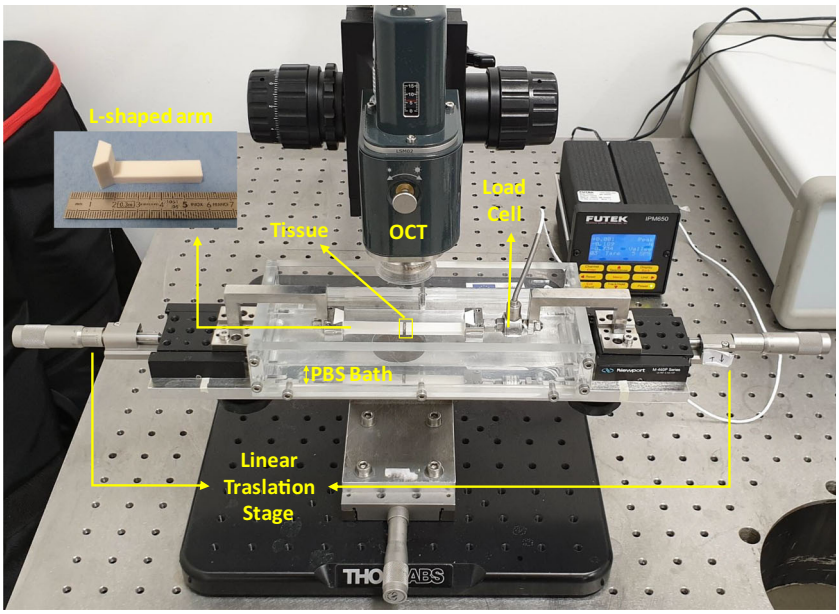

Fig. 2 Experimental setup used for radial tensile test

reported refractive index of 1.33. Optimal OCT parameters were taken from a previous study by Santamaria et al. [42]: 5 μm pixel size, 2x2mm field of view (FOV). A volume of $2\times2\times1$ mm^3 was acquired, but signal was obtained only up to a depth of 0.5 mm due to the scattering effects.

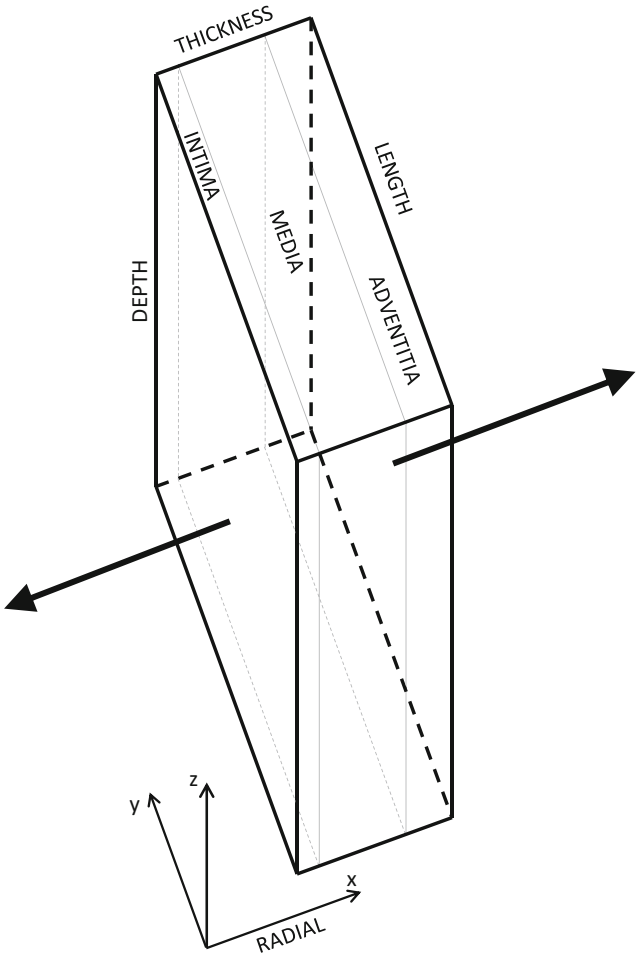

Fig. 3 Reference frame of the radial tensile test

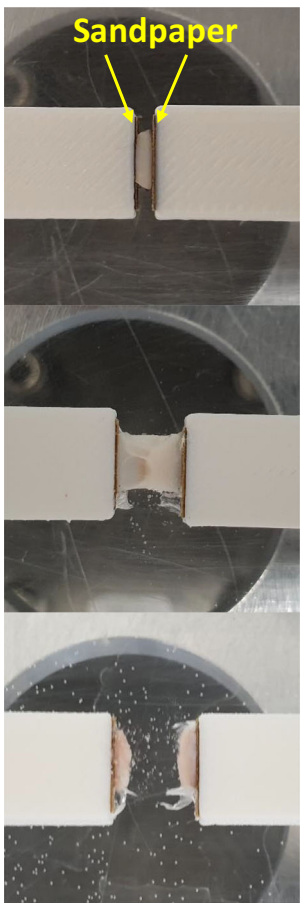

Fig. 4 Representative photographs of the initial, failure and final stage of a successful radial tensile test

During experiments, the OCT illumination tube was immersed in the PBS bath. The OCT x-y plane acquisition data were saved in TIFF stack format. The TIFF virtual stack was processed using ImageJ® software. Maximum intensity projection (MIP) [45] was applied on the stack to obtain a single representative 2D image for each step of the test. The contrast was enhanced by equalizing the histogram and the final images were exported as TIFF files for the displacement and strain measurements (Fig. 5).

Digital Image Correlation

DIC is based on the analysis of the evolution in the greyscale distribution of the images obtained at different stages of the mechanical test. In this work, the subset-based DIC algorithm implemented in Ncorr [46] was used to obtain the in-plane displacement and strain fields over a region of interest (ROI) of about 1.5 × 1.5 mm^2 at a 200 pixels/mm magnification. The selected rectangular ROI was defined to include the whole thickness of the sample. The settings used for DIC analyses [47] are given in Table 1. The E_{xx} component of the Green-Lagrangian strain tensor was finally evaluated in Ncorr according to:

$$E_{xx} = \frac{1}{2}\left[2\frac{\partial u}{\partial x} + \left(\frac{\partial u}{\partial x}\right)^2 + \left(\frac{\partial v}{\partial x}\right)^2\right]$$

Results

Figure 6 shows experimental raw and fitted data obtained by mechanical testing of all the healthy porcine samples. In the curves of Fig. 6(a) and (c), we report the points at which images were acquired for evaluating displacement (along the x direction) and strain (E_{xx} component) fields as shown in Figs. 7 and 8.

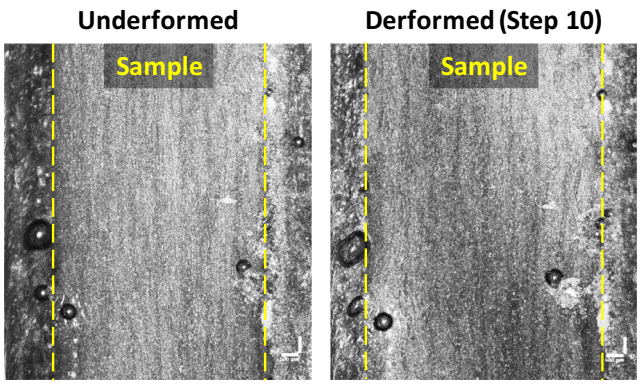

Fig. 5 Images used for DIC analysis of an undeformed and deformed porcine sample

Table 1 Setting used in the DIC analysis

DIC Settings	Value
Subset size [pixels]	30
Step size [pixels]	1
Strain window size [data points]	5
Interpolation	Biquintic B-spline
Shape function	First-order

For porcine samples, stress-strain curves were almost linear (up to the dotted lines in Figs. 6(b)-(d)-(f)-(h)-(j)) for the first steps. This was followed by a plateau region. Raw data show a stress peak at every step followed by a drop and a small valley. This behavior shows a moderate relaxation phenomenon which may be induced by chemoelastic effects in the arterial tissue as observed by [42].

Figures 7 and 8 show displacement and strain fields obtained by DIC on two porcine samples. These samples showed a strain localization with two different distributions of strain field. One presented a single localization of strain on a wide deformed area covering almost the whole thickness of the sample (Fig. 7), while the other presented a narrow deformed area not covering the whole tissue thickness and with two parallel peaks in the center of the analyzed sample (Fig. 8).

It is interesting to notice that some samples ruptured in two steps (two parallel cracks, one occurring earlier than the other), showing stress-strain curves as the one in Fig. 6(c)-(d). Indeed, it can be observed in Fig. 8 that there are 2 bands of localized strain for this sample, each one leading to a crack.

Figures 9 and 10 show displacement and strain fields obtained on two human aneurysmal samples. These two samples exhibited similar patterns of displacement and strain fields: the displacement fields show a discontinuity located into the intimal side of the first sample (Fig. 9) and in the middle of the second sample (Fig. 10). At these locations, the strain fields show peaks extending over a very narrow single area, showing a pronounced localization.

Average strains measured by DIC during the elastic range and the related stiffness values are reported in Table 2.

Discussion

Aortic samples subjected to radial tension exhibited only a limited elastic response (strains<0.05), followed by sharp strain localization during the softening response, and eventually crack initiation. Unlike the elastic response in the circumferential direction which is known to be highly nonlinear due to increased collagen recruitment [48], the elastic response in the radial direction is nearly linear given the very narrow elastic range. Nevertheless, the measured radial stiffness values

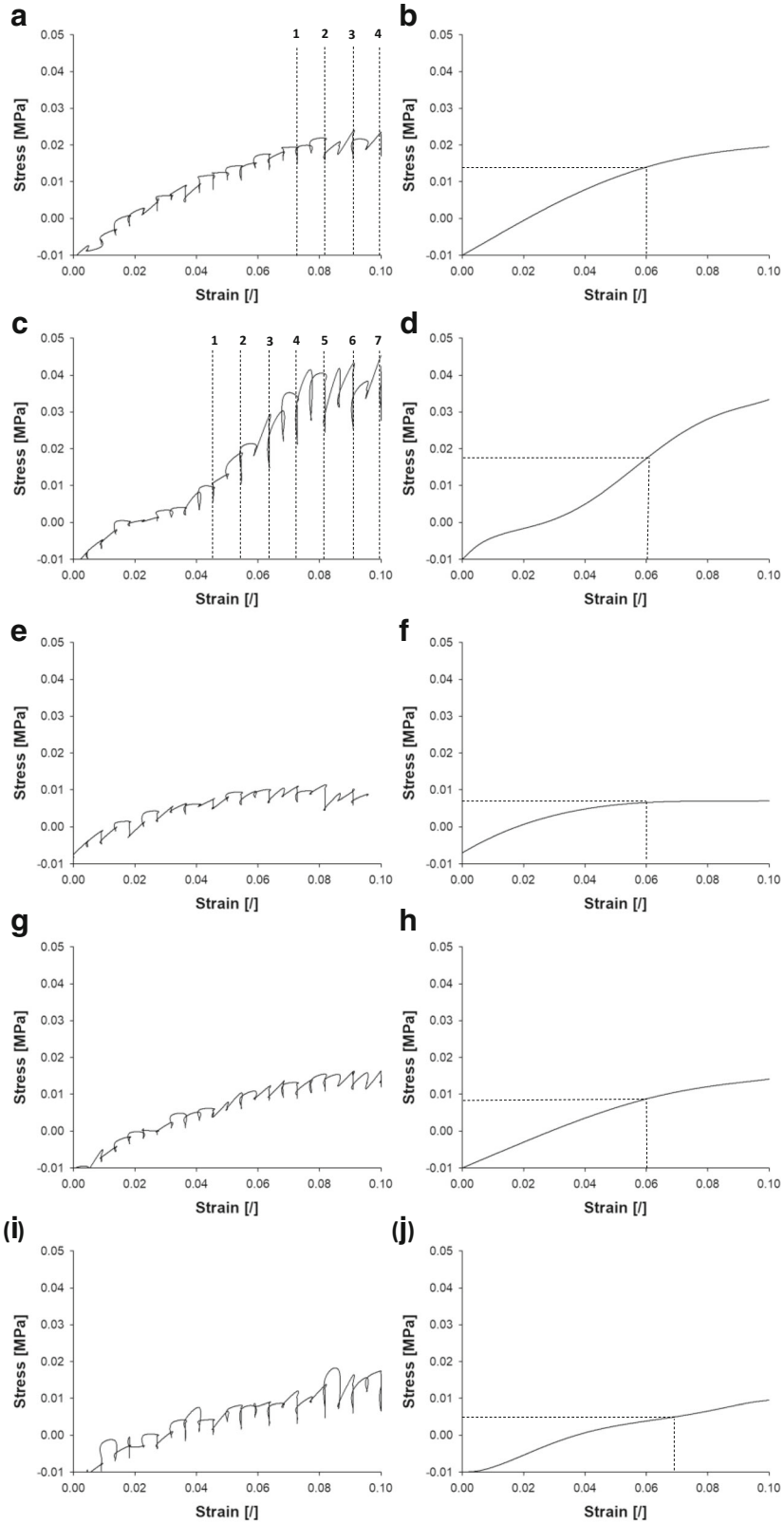

Fig. 6 Raw and fitted stress-strain data from porcine samples showing: points of raw curves corresponding to the images used for DIC and the linear part of fitted curves used for stiffness evaluation

(average: 559 ± 264 kPa) are similar to the circumferential incremental modulus reported for the same porcine aortic tissue, which was estimated to be averagely 700 kPa [44],

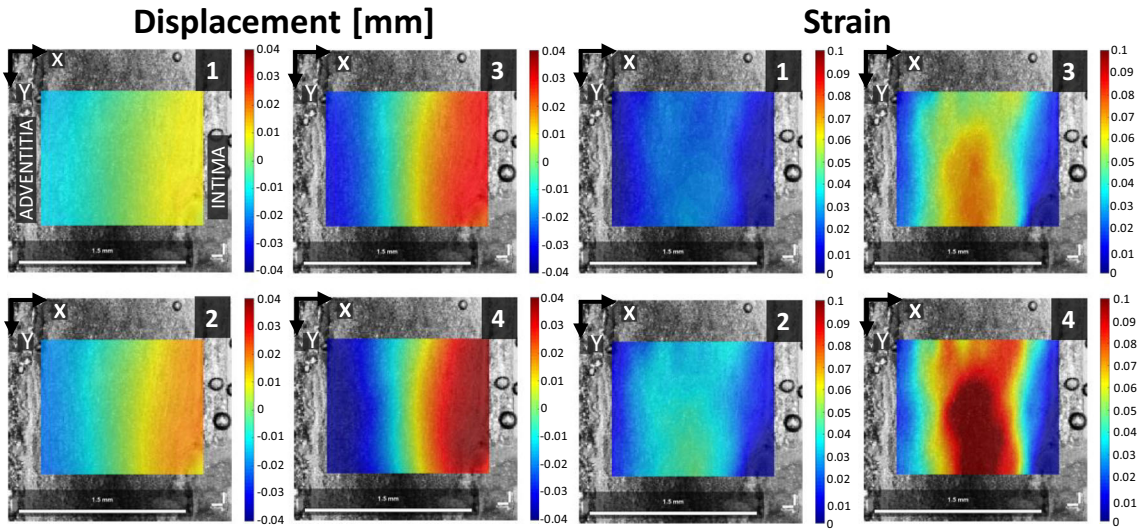

Fig. 7 Displacement (along the x direction) and strain fields (E_{xx} component) obtained by DIC on porcine sample n°1; in this particular case, the damage of the sample already reached a high value earlier after the 4th step and the strains and distortions were too high in further steps, inducing failure of the DIC

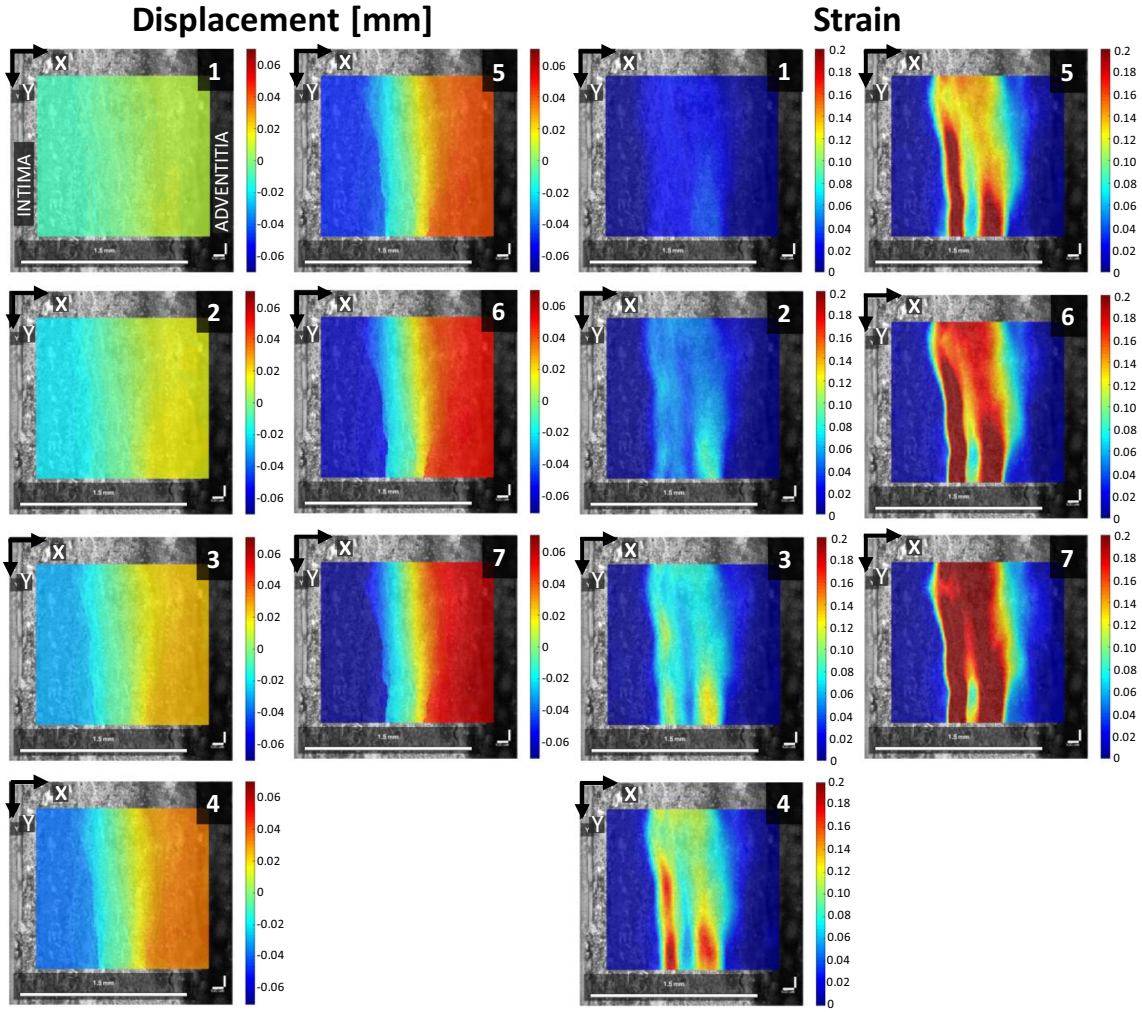

Fig. 8 Displacement (along the x direction) and strain fields (E_{xx} component) obtained by DIC on porcine sample n°2

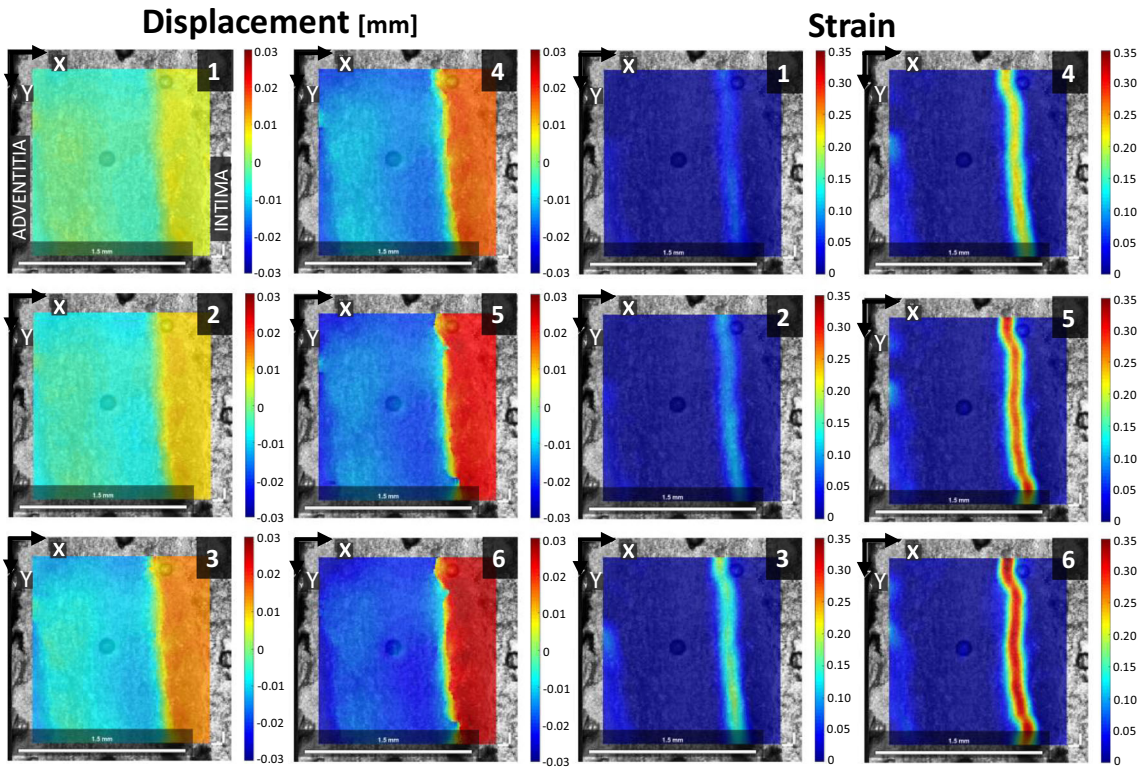

Fig. 9 Displacement (along the x direction) and strain fields (E_{xx} component) obtained by DIC on human sample n°1

and for the human aorta in the diastolic-to-systolic range which was estimated to be approximately 500 kPa [49].

Several studies investigated dissection properties of the aortic wall using different mechanical tests such as peeling test [18, 21], in-plane shear test [19, 22], and radial tensile

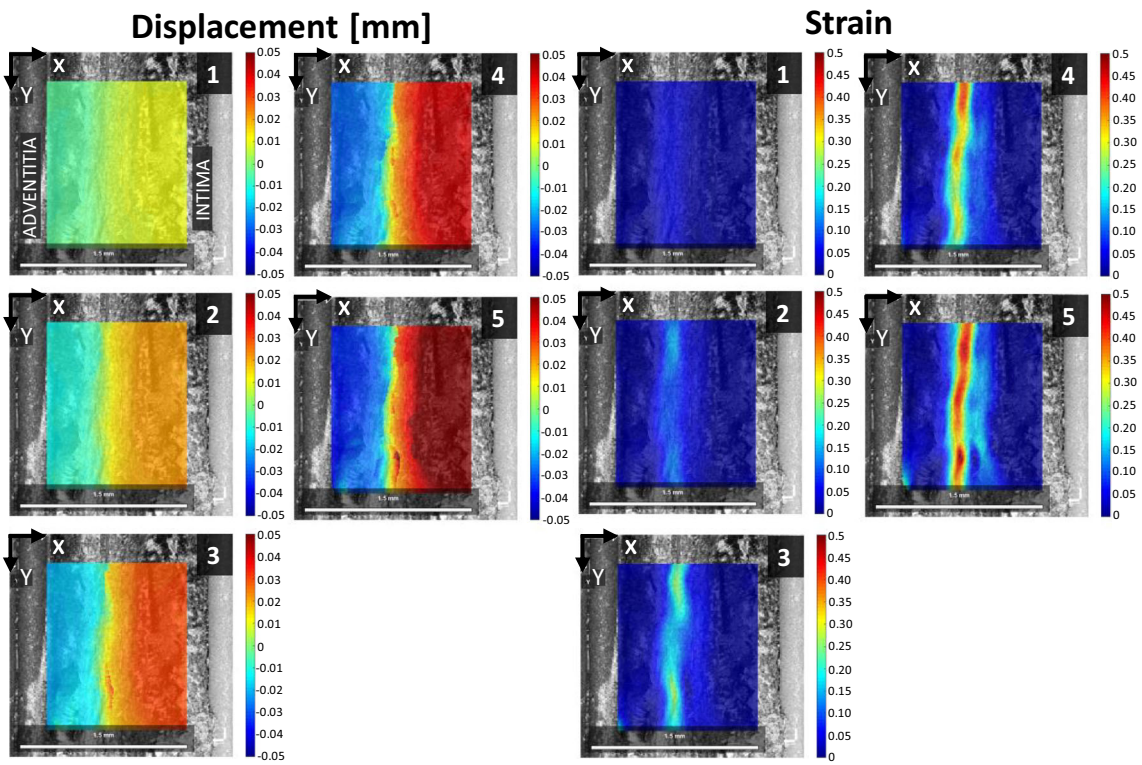

Fig. 10 Displacement (along the x direction) and strain fields (E_{xx} component) obtained by DIC on human sample n°2

Table 2 Radial stiffness values evaluated for porcine samples

Sample	Displacement applied [mm]	Average strain measured by DIC [/]	Stiffness [kPa]
#1	0.04	0.009	475
#2	0.04	0.011	288
#3	0.04	0.006	864
#4	0.04	0.011	812
#5	0.04	0.013	358
	0.04 ± 0	0.01 ± 0.003	559 ± 264

tests [18, 20]. Mechanical tests were also accompanied by histological [18, 20] or microscopic imaging investigations [21, 22].

Although these studies have well established the strength values of the aortic wall when subjected to dissection loading, the mechanisms of rupture initiation and propagation were not addressed. Here we measured displacement and strain fields during the early stage of failure to better understand the mechanism underlying AD. The use of DIC, which requires a speckle pattern on the area of interest, was possible after overcoming a number of technical issues related to the dimension of the analyzed surface. The solution was provided by combining OCT with DIC to obtain displacements and strains. OCT does not require to generate a speckle pattern in the tissue sample surface, as the optical signature of the sample creates the pattern. This is due to the ability of OCT to differentiate the composition and structure of soft tissues as the reflectivity of the tissue creates a speckle to be correlated by a correlation algorithm [50]. However, noise effects can easily corrupt the correlation for large deformations, but this was avoided by cautiously applying sequentially small loading steps during loading.

From OCT data, it is technically feasible to evaluate the strain field of the whole volume imaged using digital volume correlation (DVC). We preferred DIC given the limited penetration depth of OCT (less than 500 μm) leading to imaging of only 25% of the tissue depth. This is not enough to fully describe the mechanical behavior of aortic tissue when subjected to radial tension. Moreover, the contrast and brightness of OCT images decrease with imaging depth, which may also result in a decreasing correlation efficiency as a function of depth. This can be avoided by tissue clearing to increase the OCT imaging contrast and depth capability, but clearing can alter the biomechanical response of the aortic wall. In this way, we decided to apply maximum intensity projection on the stack of images before correlating them with the DIC algorithm.

According to DIC analysis, both healthy and pathological tissues exhibited a very early strain localization. The development of rupture in healthy aortic porcine samples was characterized by a concentration of strain localized on one or two sections of the tissue. In contrast, TAA tissue samples exhibited a sharper concentration of strain localized in a very narrow area of the aortic tissue. This difference could be explained by biomechanical weakening of the aortic wall associated with aortic dilation, but we are actually performing tests on more TAA samples to verify if there is always an aneurysmal effect on the radial tension response. Indeed, collagen fibers are the main load bearing structures in the arterial wall at large deformation while elastin bears most of the stress at small deformation. For aneurysmal tissues, the contribution of the elastin network is very small, because elastin is usually fractured in such diseased tissues [51]. This different resistance to aortic dissection of aneurysmal aorta compared to non-aneurysmal one was previously reported by Pasta et al. [21] using peeling tests.

The stress-strain curves obtained in this study for healthy porcine samples revealed an almost linear elastic behavior characterized by small strain levels. Indeed, the elastic range in the radial direction is narrow with a peak strain of 0.05, approximately. For the human aorta, tissue samples can be easily stretched upon 0.4 strain in circumferential and longitudinal directions under uniaxial tensile testing conditions. This narrow elastic range in the radial direction was previously observed by Sommer et al. [18] using a similar experimental test modality. The linear elastic part is followed by a plateau (indicating the initiation and propagation of the dissection), suggesting that the dissection may not begin and propagate at a steady rate but more in a discontinuous fashion, arresting and eventually reinitiating at regular intervals as observed in previous studies [18, 21, 52]. Vaishnav et al. [53] showed that radial properties of canine aortic walls under compression loading conditions are different from those obtained in circumferential and longitudinal directions. In healthy human aortas, MacLean et al. [20] demonstrated that radial stresses are apparently compressive, but radial tensile forces may manifest to determine the onset of dissection under certain pathological conditions.

Repeating the same methodology on tissues with different pathologies could help to decipher the conditions leading to decrease dissection resistance in the aortic wall. Moreover, since early strain localization always precedes dissection, it is suggested that delaying this strain localization could increase the resistance to dissection. The localization

phenomena could be investigated more thoroughly by finite-element analyses in the future and a failure criterion could be calibrated against the radial tensile results presented in the current study.

Limitations

The analysis was performed on samples coming from one healthy porcine aorta and one pathological human aorta so that a larger number of experiments are necessary to confirm findings. Analysis of human samples was preliminary, the purpose of this study was to introduce the method, provide a proof of concept on porcine aortas and show the possibility of extracting results for human aortas.

Storage of tissues at −24 °C and the use of glue may alter the biomechanical properties of aortic tissue prior to testing and their effect on stress-strain curves should be quantified. Gluing duration of 10 min was chosen because it was the minimum time needed to effectively cure the glue without having dry effects on the sample. We did not observe any drying effects, but further investigation may be needed for clarification on this point. About 10 other samples failed in the glue during the test (cohesive rupture), and we discarded them for this study.

Limited penetration depth of OCT on aortic tissues prevented the acquisition of complete 3D images and consequently the analysis of trough-the-thickness strain field. Given the relatively low spatial resolution of OCT images and the dimension of subset used in DIC analysis, it is possible that the separation between tissue portions would lead to an erroneous peak value of strain. Future work will adopt other DIC algorithms to deal with discontinuity in the displacement field [54]. Given the large deformation gradients, a second order shape function could more appropriately describe the displacement field and allow obtaining more accurately results.

After each displacement step the sample was no longer deformed during about 30 s to acquire the OCT images. Although there is some relaxation during this phase (force decrease), we assume there is no deformation in the sample itself (no creep) and then that the acquisition time will not affect the results. This assumption could be partially verified. Indeed, if the sample deformed during this phase, we would observe spurious effects in the OCT images and strain maps related to the scanning process. Indeed, OCT scans the sample, raw after raw, starting from top left and finishing at bottom right. We never observed gradients related to this scanning process in the strain maps. However, we admit that the acquisition time should be reduced.

It was not possible to precondition the tissue because even a small strain could cause a damage in the tissue. Previous studies achieving similar tests [55] did not report preconditioning either.

Finally, we are aware that dissections are multifactorial and that radial tension is not the only factor that can explain dissection, but it is important to understand how arteries respond to radial tension to better understand how dissections can initiate.

Conclusions

In conclusion, we developed a new methodology to evaluate strain fields during dissection tests by combining OCT imaging with DIC. This methodology was applied to radial tensile tests carried out on healthy and pathological aortic tissues. Aortic tissues showed an early localization of strain, with the healthy animal aortic tissue showing strain localized on one or two sections and the pathological human aortic tissue having a sharper strain localization. This different mechanical behavior may be an expression of a weakened aortic wall in TAA but future studies using the proposed OCT combined with DIC are needed to better understand the mechanisms underlying strain localization related to dissection. We submit that repeating the methodology presented on tissues collected from patients with different pathological conditions can highlight in which conditions the resistance to dissection would decrease and what may explain this resistance at the tissue level.

Acknowledgments The authors want to thank Katia Genovese for her insight in this work.

Compliance with Ethical Standards

Conflict of Interest The authors declare that there is no conflict of interest regarding the publication of this article.

Stéphane Avril is grateful to the European Research Council (ERC grant Biolochanics, grant number 647067) for financial support. This work was supported by a “Ricerca Finalizzata” grant from the Italian Ministry of Health (GR-2011-02348129) to Salvatore Pasta, and by grant from PON FSE-FESR Ricerca Innovazione 2014–2020 to Marzio Di Giuseppe.

The Veterinary School of Lyon (Institut Claude Bourgelat) supplied the aortas in accordance with the recommendations of the ethics committee of VetAgro Sup (C2EA No 18) and animal testing regulation – Directive 2010/63/EU. The study and protocol were reviewed and approved by the ethics committee of VetAgro Sup (project approved under No 1546).

The collection of the ATAA tissue was carried out in accordance with guidelines of the Institutional Review Board of the University Hospital Center of Saint-Etienne, and the patient signed informed consent before surgery.

References

1. Khan IA, Nair CK (2002) Clinical, diagnostic, and management perspectives of aortic dissection. Chest 122(1):311–328. https://doi.org/10.1378/chest.122.1.311
2. Mikich B (2003) Dissection of the aorta: a new approach. Heart 89(1):6–8. https://doi.org/10.1136/heart.89.1.6
3. Criado FJ (2011) Aortic dissection: a 250-year perspective. Tex Heart Inst J 38(6):694–700
4. Oberwalder PJ (2001) Aneurysms and dissection of the thoracic aorta: definition and pathology. Journal fur Kardiologie 8(1–2):2–4
5. Kouchoukos NT, Dougenis D (1997) Surgery of the thoracic aorta. N Engl J Med 336(26):1876–1889
6. van Baardwijk C, Roach MR (1987) Factors in the propagation of aortic dissections in canine thoracic aortas. J Biomech 20(1):67–73
7. Tam AS, Sapp MC, Roach MR (1998) The effect of tear depth on the propagation of aortic dissections in isolated porcine thoracic aorta. J Biomech 31(7):673–676
8. Wolinsky H, Glagov S (1967) A lamellar unit of aortic medial structure and function in mammals. Circ Res 20(1):99–111
9. Auer J, Berent R, Eber B (2000) Aortic dissection: incidence, natural history and impact of surgery. J Clin Basic Cardiol 3(3):151–154
10. Elefteriades JA, Farkas EA (2010) Thoracic aortic aneurysm: clinically pertinent controversies and uncertainties. J Am Coll Cardiol 55(9):841–857. https://doi.org/10.1016/j.jacc.2009.08.084
11. Elefteriades JA (2008) Thoracic aortic aneurysm: reading the enemy's playbook. Curr Probl Cardiol 33(5):203–277
12. Trimarchi S, Jonker FH, Froehlich JB, Upchurch GR, Moll FL, Muhs BE, Rampoldi V, Patel HJ, Eagle KA, investigators IRoAAD (2012) Acute type B aortic dissection in the absence of aortic dilatation. J Vasc Surg 56 (2):311–316
13. Geest JPV, Wang DH, Wisniewski SR, Makaroun MS, Vorp DA (2006) Towards a noninvasive method for determination of patient-specific wall strength distribution in abdominal aortic aneurysms. Ann Biomed Eng 34(7):1098–1106
14. Azadani AN, Chitsaz S, Mannion A, Mookhoek A, Wisneski A, Guccione JM, Hope MD, Ge L, Tseng EE (2013) Biomechanical properties of human ascending thoracic aortic aneurysms. Ann Thorac Surg 96(1):50–58
15. Pasta S, Agnese V, Di Giuseppe M, Gentile G, Raffa GM, Bellavia D, Pilato M (2017) *In vivo* strain analysis of dilated ascending thoracic aorta by ECG-gated CT angiographic imaging. Ann Biomed Eng 45(12):2911–2920
16. Pasta S, Gentile G, Raffa G, Bellavia D, Chiarello G, Liotta R, Luca A, Scardulla C, Pilato M (2017) In silico shear and intramural stresses are linked to aortic valve morphology in dilated ascending aorta. Eur J Vasc Endovasc Surg 54(2):254–263
17. Rinaudo A, D'Ancona G, Lee JJ, Pilato G, Amaducci A, Baglini R, Follis F, Pilato M, Pasta S (2014) Predicting outcome of aortic dissection with patent false lumen by computational flow analysis. Cardiovasc Eng Technol 5(2):176–188
18. Sommer G, Gasser TC, Regitnig P, Auer M, Holzapfel GA (2008) Dissection properties of the human aortic media: an experimental study. J Biomech Eng 130(2):021007
19. Haslach HW Jr, Gipple J, Taylor B, Rabin J (2018) Comparison of aneurysmal and non-pathologic human ascending aortic tissue in shear. Clin Biomech 58:49–56
20. MacLean NF, Dudek NL, Roach MR (1999) The role of radial elastic properties in the development of aortic dissections. J Vasc Surg 29(4):703–710
21. Pasta S, Phillippi JA, Gleason TG, Vorp DA (2012) Effect of aneurysm on the mechanical dissection properties of the human ascending thoracic aorta. J Thorac Cardiovasc Surg 143(2):460–467
22. Sommer G, Sherifova S, Oberwalder PJ, Dapunt OE, Ursomanno PA, DeAnda A, Griffith BE, Holzapfel GA (2016) Mechanical strength of aneurysmatic and dissected human thoracic aortas at different shear loading modes. J Biomech 49(12):2374–2382
23. Ahmadzadeh H, Rausch M, Humphrey J (2019) Modeling lamellar disruption within the aortic wall using a particle-based approach. Sci Rep 9(1):1–17
24. Roccabianca S, Ateshian GA, Humphrey JD (2014) Biomechanical roles of medial pooling of glycosaminoglycans in thoracic aortic dissection. Biomech Model Mechanobiol 13(1):13–25
25. Yang Y, Dubois A, X-p Q, Li J, El Haj A, Wang RK (2006) Investigation of optical coherence tomography as an imaging modality in tissue engineering. Phys Med Biol 51(7):1649–1659
26. Huang Y-P, Zheng Y-P, Wang S-Z, Chen Z-P, Huang Q-H, He Y-H (2008) An optical coherence tomography (OCT)-based air jet indentation system for measuring the mechanical properties of soft tissues. Meas Sci Technol 20(1):015805
27. Mahdian M, Salehi HS, Lurie AG, Yadav S, Tadinada A (2016) Tissue characterization using optical coherence tomography and cone beam computed tomography: a comparative pilot study. Oral Surg Oral Med Oral Pathol Oral Radiol 122(1):98–103
28. Real E, Eguizabal A, Pontón A, Díez MC, Val-Bernal JF, Mayorga M, Revuelta JM, López-Higuera JM, Conde OM (2013) Optical coherence tomography assessment of vessel wall degradation in thoracic aortic aneurysms. J Biomed Opt 18(12):126003
29. Tucker-Schwartz J, Skala M (2012) Contrast enhancement in optical coherence tomography. Citeseer
30. Huang D, Swanson EA, Lin CP, Schuman JS, Stinson WG, Chang W, Hee MR, Flotte T, Gregory K, Puliafito CA et al (1991) Optical coherence tomography. Science (New York, NY) 254(5035):1178–1181. https://doi.org/10.1126/science.1957169
31. Rogowska J, Patel N, Fujimoto J, Brezinski M (2004) Optical coherence tomographic elastography technique for measuring deformation and strain of atherosclerotic tissues. Heart 90(5):556–562
32. Palanca M, Tozzi G, Cristofolini L (2016) The use of digital image correlation in the biomechanical area: a review. Int Biomech 3(1):1–21
33. Fu J, Pierron F, Ruiz PD (2013) Elastic stiffness characterization using three-dimensional full-field deformation obtained with optical coherence tomography and digital volume correlation. J Biomed Opt 18(12):121512
34. Chu T, Ranson W, Sutton MA (1985) Applications of digital-image-correlation techniques to experimental mechanics. Exp Mech 25(3):232–244
35. Pan B, Qian K, Xie H, Asundi A (2009) Two-dimensional digital image correlation for in-plane displacement and strain measurement: a review. Meas Sci Technol 20(6):062001
36. Sutton MA, Orteu JJ, Schreier H (2009) Image correlation for shape, motion and deformation measurements: basic concepts, theory and applications. Springer Science & Business Media
37. Bruck H, McNeill S, Sutton MA, Peters W (1989) Digital image correlation using Newton-Raphson method of partial differential correction. Exp Mech 29(3):261–267
38. Bersi MR, Bellini C, Di Achille P, Humphrey JD, Genovese K, Avril S (2016) Novel methodology for characterizing regional variations in the material properties of murine aortas. J Biomech Eng 138(7):071005
39. Genovese K, Montes A, Martinez A, Evans SL (2015) Full-surface deformation measurement of anisotropic tissues under indentation. Med Eng Phys 37(5):484–493

40. Lecompte D, Smits A, Bossuyt S, Sol H, Vantomme J, Van Hemelrijck D, Habraken A (2006) Quality assessment of speckle patterns for digital image correlation. Opt Lasers Eng 44(11):1132–1145
41. Trabelsi O, Davis FM, Rodriguez-Matas JF, Duprey A, Avril S (2015) Patient specific stress and rupture analysis of ascending thoracic aneurysms. J Biomech 48(10):1836–1843
42. Acosta Santamaría VA, Flechas García M, Molimard J, Avril S (2018) Three-dimensional full-field strain measurements across a whole porcine aorta subjected to tensile loading using optical coherence tomography–digital volume correlation. Front Mech Eng 4:3
43. Wang RK (2002) Tissue clearing as a tool to enhance imaging capability for optical coherence tomography. In: Coherence Domain Optical Methods in Biomedical Science and Clinical Applications VI. International Society for Optics and Photonics, pp 22–25
44. Santamaría VAA, García MF, Molimard J, Avril S (2020) Characterization of chemoelastic effects in arteries using digital volume correlation and optical coherence tomography. Acta Biomater 102:127–137
45. Prokop M, Shin HO, Schanz A, Schaefer-Prokop CM (1997) Use of maximum intensity projections in CT angiography: a basic review. Radiographics 17(2):433–451
46. Blaber J, Adair B, Antoniou A (2015) Ncorr: open-source 2D digital image correlation matlab software. Exp Mech 55(6):1105–1122
47. Reu P (2015) The art and application of DIC. Exp Tech
48. Sokolis DP, Kefaloyannis EM, Kouloukoussa M, Marinos E, Boudoulas H, Karayannacos PE (2006) A structural basis for the aortic stress–strain relation in uniaxial tension. J Biomech 39(9):1651–1662
49. Avril S (2019) Aortic and arterial mechanics. arXiv preprint arXiv:191206408
50. Sun C, Standish BA, Vuong B, Wen X-Y, Yang VX (2013) Digital image correlation–based optical coherence elastography. J Biomed Opt 18(12):121515
51. Tong J, Schriefl AJ, Cohnert T, Holzapfel GA (2013) Gender differences in biomechanical properties, thrombus age, mass fraction and clinical factors of abdominal aortic aneurysms. Eur J Vasc Endovasc Surg 45(4):364–372
52. Purslow P (1983) Measurement of the fracture toughness of extensible connective tissues. J Mater Sci 18(12):3591–3598
53. Vaishnav RN, Young JT, Janicki JS, Patel DJ (1972) Nonlinear anisotropic elastic properties of the canine aorta. Biophys J 12(8):1008–1027
54. Réthoré J, Hild F, Roux S (2008) Extended digital image correlation with crack shape optimization. Int J Numer Methods Eng 73(2):248–272
55. Sommer G, Gasser TC, Regitnig P, Auer M, Holzapfel GA (2008) Dissection properties of the human aortic media: an experimental study. J Biomech Eng 130(2)